Added Value of SPECT/CT Fusion in Assessing Suspected Bone Metastasis: Comparison with Scintigraphy Alone and Nonfused Scintigraphy and CT[1]

Daisuke Utsunomiya, MD
Shinya Shiraishi, MD
Masanori Imuta, MD
Seiji Tomiguchi, MD
Koichi Kawanaka, MD
Shoji Morishita, MD
Kazuo Awai, MD
Yasuyuki Yamashita, MD

Purpose: To evaluate retrospectively if there is additional diagnostic value of fused single photon emission computed tomographic (SPECT) and computed tomographic (CT) images in assessing possible bone metastases.

Materials and Methods: Institutional review board approval was obtained, and each patient provided written informed consent. Bone scintigraphy—including planar and SPECT imaging—and CT were performed with a combined SPECT/CT system in 45 oncologic patients (24 men, 21 women; mean age, 64.7 years $\pm$ 8.7), with a total of 42 metastatic bone foci and 40 benign foci. The reference standard was follow-up radiologic imaging. Two independent readers first analyzed only bone scintigraphic images and next analyzed two separate sets of bone scintigraphic and CT images. They then analyzed bone scintigraphic, CT, and fused images and focused on the additional value of fused images. Diagnostic confidence for each lesion was scored. The three analyses were performed 7 days apart, and the images were presented in random order at each session. The value of additional fused images was assessed by using receiver operating characteristic analysis.

Results: After review of fused images to classify indeterminate lesions, reviewer 1 became more confident in diagnosis of the 15 benign lesions and two metastases, and reviewer 2 became more confident in diagnosis of the seven benign lesions and one metastasis. The area under the receiver operating characteristic curve for reviewer 1 was 0.589 for scintigraphic images, 0.831 for separate data sets of scintigraphic and CT images, and 0.947 for fused images. The corresponding areas under the receiver operating characteristic curve for reviewer 2 were 0.771, 0.885, and 0.968, respectively.

Conclusion: Results demonstrate the increased diagnostic confidence obtained with fused SPECT/CT images compared with separate sets of scintigraphic and CT images in differentiating malignant from benign bone lesions.

© RSNA, 2005

Radiology

Metastases to bone are unfortunately common (1,2), and the frequency with which they are detected varies considerably with the method used (1). Positron emission tomography (PET) with fluorine 18 fluorodeoxyglucose, or FDG, has proved to be successful for imaging various malignant neoplasms, although bone scintigraphy might be superior to FDG PET in the detection of bone metastasis (1–8). However, bone scintigraphy lacks specificity (1–3). Precise anatomic localization of the radiotracer uptake may clarify the nature of the abnormality (2–4,9). This localization can be achieved by means of image fusion between single photon emission computed tomography (SPECT) and computed tomography (CT) (10–14). Image fusion is an exciting area of study in which there is the potential to positively influence patient care, particularly in patients with cancer (11,13). In clinical practice, however, image fusion may be difficult to achieve because it requires various steps (image transfer, reading, registration, and reslicing) that are not optimized for all parts of the body and are usually time consuming (10,15). Current anatomic images may not be available at the time of the nuclear medicine procedure (10). In addition, even with external fiducial markers, registration errors of functional and anatomic data obtained separately with different devices may occur as a result of variations in patient positioning (16,17).

Recently, PET/CT has been introduced (18), but SPECT might be valuable for clinical diagnosis in many circumstances (6–8,19–23). An anatomic x-ray transmission system mounted on a gamma camera has been introduced (10). The x-ray-tube–based CT system, however, has poor performance, and the lower-resolution anatomic images (approximately 4 mm) may often be insufficient for image interpretation. To create a robust mode for inherent registration between SPECT and high-resolution CT images (approximately 0.7 mm), we have designed an imaging system that combines a dual-head, gantry-free gamma camera with a multi–detector row CT system; this imaging system allows correct fusion of images without the need to change the patient's position. Few studies have compared the diagnostic accuracy of combined SPECT/CT fusion and side-by-side reading of SPECT and CT data. Thus, the purpose of our study was to evaluate retrospectively if there is additional diagnostic value in fused SPECT and CT images for the assessment of possible bone metastases.

Materials and Methods

Patients

From information acquired in our radiologic database between October 2002 and August 2003, we retrospectively reviewed bone scintigrams, including planar and SPECT images, and helical CT images from 45 various oncologic patients (24 men and 21 women; age range, 44–76 years; mean age, 65 years) who had been examined with our combined SPECT/CT system (Table 1). All patients had been referred to our department (Kumamoto Regional Medical Center, Kumamoto, Japan) for the investigation of bone metastasis and met the following criteria: (a) presence of a histologically proved cancer but no known bone metastasis and (b) presence of four or fewer foci of abnormal
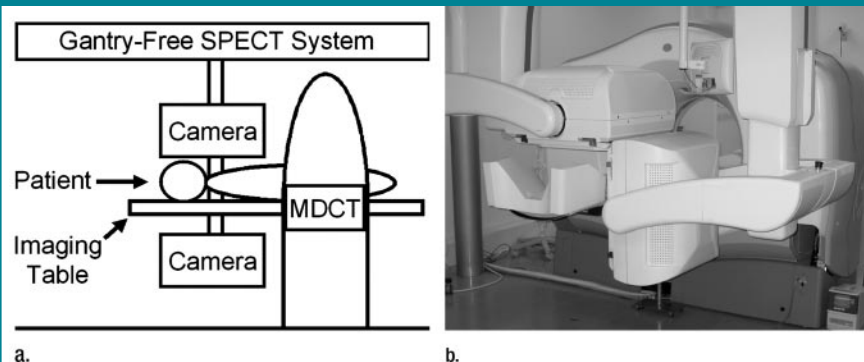
Table 1

Malignancy Types among 45 Patients

Malignancy Type	No. of Patients
Prostate cancer	9 (20)
Breast cancer	9 (20)
Lung cancer	7 (16)
Hepatocellular carcinoma	5 (11)
Colon and rectal carcinoma	4 (9)
Pancreatic cancer	4 (9)
Renal cell carcinoma	3 (7)
Thyroid cancer	2 (4)
Osteosarcoma	1 (2)
Nasopharyngeal carcinoma	1 (2)

Note.—Numbers in parentheses are percentages.

Figure 1

Figure 1: **(a)** Schematic and **(b)** photograph of combined SPECT/CT system. SPECT and CT *(MDCT)* scanners are adjacent, which obviates repositioning of patient because the CT patient table extends into gantry-free SPECT system.
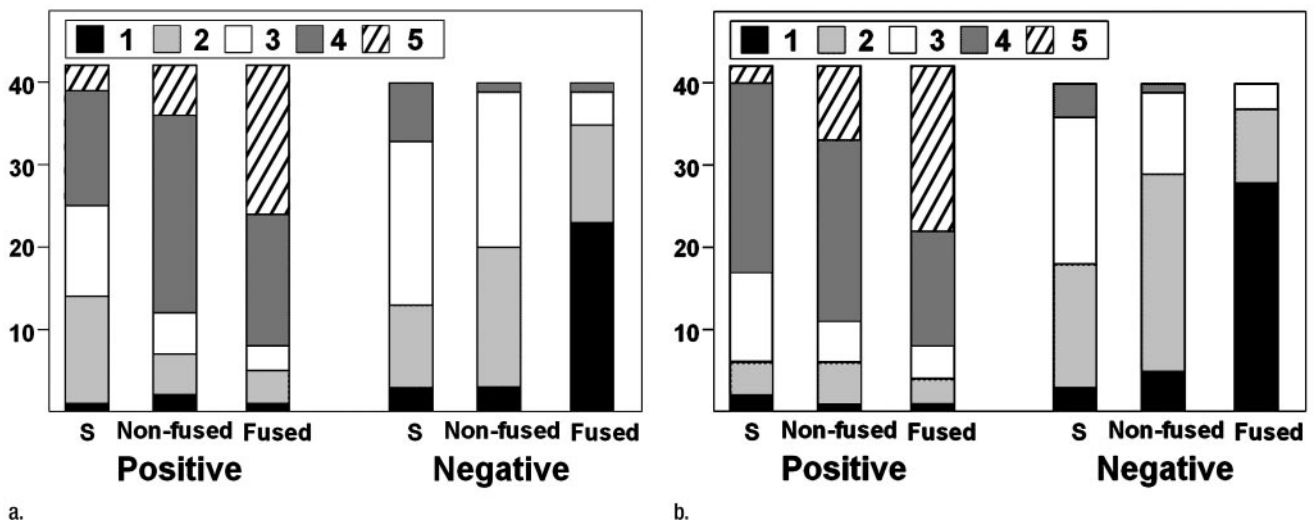
Figure 2

a.

b.

Figure 2: Diagnostic confidence scores of three reviews each for reviewers **(a)** 1 and **(b)** 2. (*1* = definitely not metastasis, *2* = probably not metastasis, *3* = indeterminate, *4* = probably metastasis, *5* = definitely metastasis.) *Fused* = fused bone scintigraphic and CT images, *Negative* = actually negative cases, *Non-fused* = separate data sets of bone scintigraphic and CT images, *Positive* = actually positive cases, and *S* = bone scintigraphic images alone.

radiotracer uptake at planar bone scintigraphy. The bone lesions were considered metastases if an increase in tumor size was confirmed with follow-up radiologic studies, including bone scintigraphy, CT, and magnetic resonance (MR) imaging, with or without exacerbation of clinical symptoms. According to these criteria, 42 lesions were considered metastatic bone foci, and 40 were considered benign foci (eg, osteoarthritis, fracture, osteophyte) in these 45 patients.

Institutional review board approval was obtained for both multiple imaging studies and retrospective review of these images. Each patient provided written informed consent for both the multiple imaging approach and the retrospective data analysis. Results of the imaging examinations were discussed with the patients, and all patient questions were answered.

System Design

The combined SPECT/CT system incorporates a gantry-free SPECT scanner (Skylight; ADAC Laboratories, Milpitas, Calif) and an eight–detector row CT scanner (LightSpeed Ultra; GE Medical Systems, Milwaukee, Wis). The two commercial devices were juxtaposed

Table 2

Tracer Uptake Sites among Malignant and Benign Lesions

	Metastases (*n* = 42)	Benign Lesions (*n* = 40)
Vertebral body	9 (21)	14 (35)
Pedicle	8 (19)	3 (7.5)
Vertebral body and pedicle	8 (19)	2 (5.0)
Facet joint	3 (7)	10 (25)
Rib	7 (17)	6 (15)
Femur	4 (10)	3 (8)
Pelvis	3 (7)	2 (5)

Note.—Numbers in parentheses are percentages.

such that the CT table could move with the patient directly into the SPECT scanner prior to CT scanning (Fig 1).

Bone Scintigraphy

Whole-body planar imaging in the anterior and posterior positions was performed 3 hours after the injection of 555 MBq (15 mCi) of technetium 99m (^{99m}Tc) methylene diphosphate or at 2 hours after the injection of 555 MBq of ^{99m}Tc–hydroxymethylene diphosphonate. Scintigraphy was performed with dual-head detectors equipped with a low-energy, general-purpose, parallel-hole collimator. On the basis of findings

on planar scintigrams, which showed a small number of abnormal foci (four or fewer), 45 patients underwent SPECT imaging 30 minutes after planar imaging. SPECT images were obtained at a magnification factor of 1.25 in a 64 × 64 matrix. Sixty-four projections were acquired at 6° intervals. The time required for acquisition of each projection was approximately 30 seconds, and the full study lasted 20 minutes. SPECT images were reconstructed with filtered backprojection, and high-frequency noise was decreased with postreconstruction Butterworth filtering (cutoff, 0.50 cycle per pixel; order, five) on a computer worksta-

tion (Pegasys; ADAC Laboratories). Attenuation correction with use of CT images was performed with software (Hyogo CM Attenuation Correction; Hyogo College of Medicine, Nishinomiya, Hyogo, Japan) (24) on the computer workstation.

CT Scanning

Unenhanced CT scanning (120 kV, 140 mA, 0.7-second per rotation, 2.5-mm collimation, and 5-mm reconstruction) was performed in the helical mode with a table speed of 17.5 mm per rotation. CT images were reconstructed with a standard reconstruction algorithm and a 512×512 matrix, 35–40-cm field of view for image fusion, and 50-cm field of view for attenuation correction.

Image Fusion: SPECT and CT

Image fusion was performed with a dedicated workstation (Dr.View; Asahikasei, Tokyo, Japan). Internal anatomic structures seen on both CT and SPECT images were used to determine the geometric transformation. Anatomic structures chosen as internal markers included bones, kidneys, and the urinary tract. Image fusion was confirmed in transverse, sagittal, and coronal planes on the computer display by means of consensus of two diagnostic radiologists (D.U., S.T.). One radiologist (D.U.) had 9 years of experience, and the other (S.T.) had 20 years of experience in both nuclear medicine and CT imaging.

Image Analysis

Images were retrospectively and independently interpreted by two board-certified radiologists (M.I., S.S.), with knowledge of the patient's history of malignancy. Reviewer 1 (M.I.) had 6 years of experience, and reviewer 2 (S.S.) had 10 years of experience in both nuclear medicine and CT imaging.

First, the reviewers read bone scintigraphic images, including planar and SPECT images. Second, 7 days later, the reviewers interpreted scintigraphic images and helical CT images separately. Third, a further 7 days later, the reviewers interpreted all three types of images, including scintigraphic images, CT images, and fused SPECT/CT images, focusing on the additional value of fused images in differentiating between benign and metastatic radiotracer uptake. The images were presented in random order to each of the readers at each session. Before the image interpretation, five training cases not included in the observer test were distributed to the observers to familiarize them with the scoring system. Each reviewer recorded his degree of confidence as to whether a site of abnormal radiotracer uptake represented a bone metastasis in each image interpretation session. Diagnostic confidence for each lesion was scored with a five-point scale: 1, definitely not metastasis; 2, probably not metastasis; 3, indeterminate; 4, probably metastasis; and 5, definitely metastasis. No time constraints were placed on the reviewers. Lesions in which diagnostic confidence was scored as 4 or 5 were counted as metastasis. Lesions in which diagnostic confidence was scored as 1 or 2 were counted as benign. We assessed whether fused images enabled reviewers to reclassify the indeterminate lesions on nonfused images. Reasons for scoring error were also assessed.

For objectivity and reproducibility of the image analysis, the criteria for classifying a bone lesion as benign or malignant were determined. The criteria for bone scintigraphy were the following: *(a)* radiotracer uptake greater than that in the anterior iliac spine was considered to indicate malignancy, and *(b)* radiotracer uptake equal to or lower than that in the anterior iliac spine and radiotracer uptake that involved both sides of the joint (eg, knees, hands, and wrists) were considered to indicate benignancy. The criteria for CT images were the following: *(a)* an osteolytic lesion with soft-tissue mass or a sharply delineated osteoblastic lesion and a lesion that showed asymmetric increased
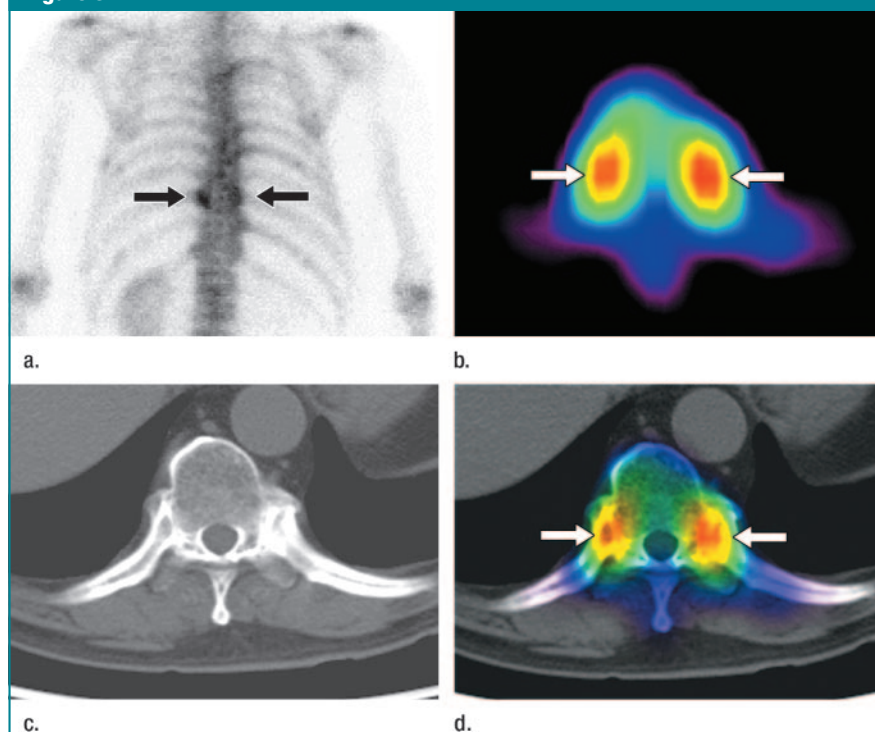

Figure 3: Images of 70-year-old man with pancreatic cancer. **(a)** Posterior planar scintigram and **(b)** transverse SPECT image show bilateral foci of increased tracer uptake in thoracic vertebra (arrows). **(c)** Transverse CT image shows no apparent bone lesion. **(d)** Transverse fused image shows precise localization of abnormal tracer uptake in articular facets of head of rib (arrows). This finding was suggestive of osteoarthritis. Later bone scans and 1 year of disease-free follow-up helped confirm the absence of bone metastasis.
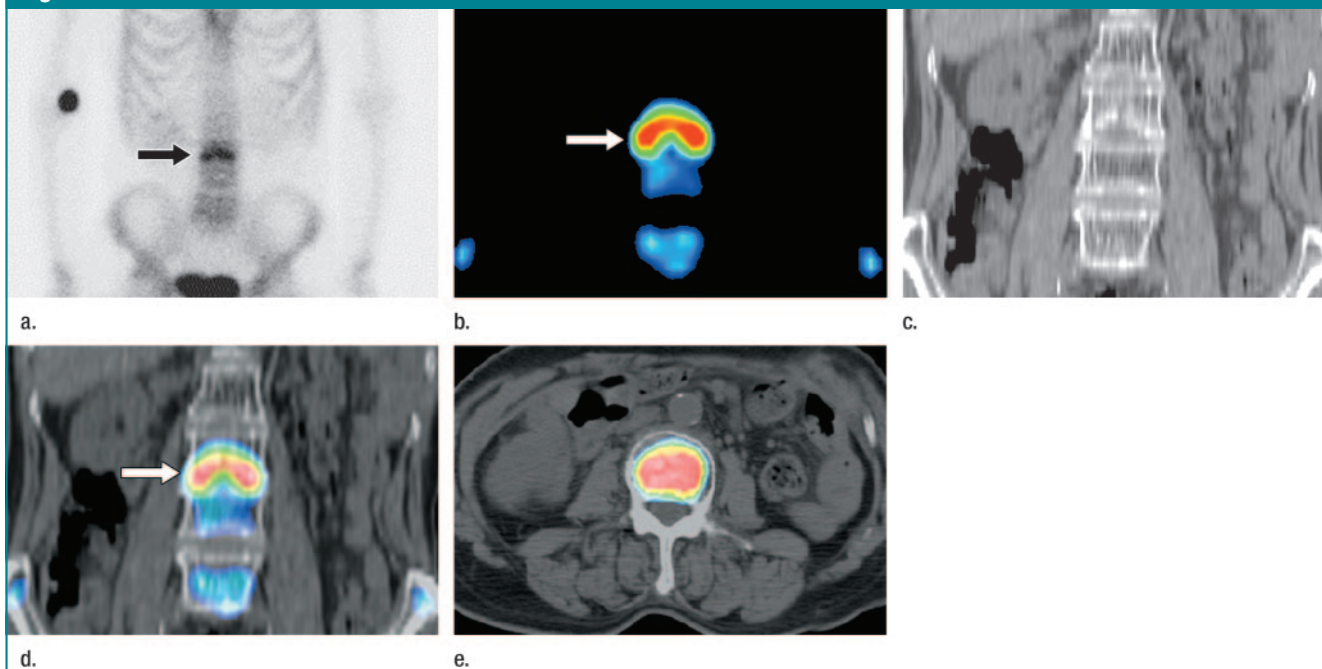
Figure 4

Figure 4: Images of 63-year-old man with prostate cancer. **(a)** Anterior planar scintigram and **(b)** coronal SPECT image show increased tracer uptake (arrow) in the lumbar vertebral body. **(c)** Coronal reformatted CT image shows compression fracture in third lumbar vertebral body. **(d)** Coronal fused image shows precise localization of abnormal tracer uptake in end plate of third lumbar vertebral body (arrow). **(e)** Transverse fused image shows no pedicle involvement. Findings on fused images were suggestive of compression fracture due to osteoporosis. Results of MR imaging and later bone scanning helped confirm the absence of bone metastasis.

density of bone marrow were considered to be malignant, and (b) a partial sclerotic lesion with angular or indistinct margin was considered to be benign (eg, osteophyte, arthritis, compression fracture). When the interpretation on bone scintigrams disagreed with that on CT images in the second review, the interpretation at bone scintigraphy was used. When accurate localization of radiotracer uptake on fused images clarified the nature of the lesion, the reviewer changed the score.

Statistical Analysis

The degree of agreement between the two reviewers was measured with the κ statistic. κ values were reported as follows: 0, agreement is a random effect; less than 0.20, poor agreement; 0.21–0.40, fair agreement; 0.41–0.60, moderate agreement; 0.61–0.80, substantial agreement; and 0.81–1.00, almost perfect agreement (25). For the calculation of κ values, SAS 8.01 for Windows (SAS Institute, Cary, NC) was used.

The value of additional information provided by fused bone scintigraphic and CT images was assessed by means of receiver operating characteristic (ROC) analysis. The index of performance for each reading session was the area under the ROC curve (A_z). The A_z value and its confidence interval was estimated with the DeLong, DeLong, and Clarke-Pearson method (26). Our study was a diagnostic assessment with patient-clustered data, and, thus, the bootstrap resampling approach with 10 000 iterations was used for estimating the bootstrap mean A_z and confidence interval (27,28). Calculation of A_z values was performed with software (AccROC 2.4; Accumetric, Motreal, Quebec, Canada). ROC curves were generated by using Rockit software (beta version 0.9.1; Charles E. Metz and Benjamin A. Herman, University of Chicago, Chicago, Ill).

Results

Image Analysis

Radiotracer uptake information is summarized in Table 2. A total of 82 areas of abnormal tracer uptake were depicted in 45 patients on planar scintigraphic images. Each reader identified all 82 lesions. Twenty patients had a single lesion, 15 had two lesions, eight had three lesions, and two had four lesions. Diagnostic confidence scores for each reviewer are shown in Figure 2.

After additional review of fused scintigraphic and CT images, reviewer 1 reclassified 17 indeterminate lesions on nonfused images as benign (15 lesions) or malignant (two lesions). Eight of these 15 benign lesions were arthritis (Fig 3), five were a compression fracture of a vertebral body (Fig 4), one was an old rib fracture, and one was degeneration of a vertebral body. Two metastatic lesions were visible as slightly sclerotic or erosive changes on CT images (Fig 5). After additional review of fused scintigraphic and CT images, reviewer 2 reclassified eight indeterminate lesions on nonfused images as benign (seven lesions) or malignant (one lesion). Four of these seven benign lesions were arthritis, one was a compression fracture of a vertebral body, one was an old rib fracture,

and one was degeneration of a vertebral body. One metastatic lesion was visible as slightly sclerotic change on CT images. Assessment of the reclassification of these indeterminate lesions showed that a review of fused images enabled reviewers to be more confident in the characterization of these lesions. For five of 42 metastatic lesions, reviewer 1 rendered a false-negative diagnosis. Three of these five lesions were undetectable on CT images, one appeared slightly sclerotic on CT images, and one was near the joint of the head of the rib. For four of 42 metastatic lesions, reviewer 2 rendered a false-negative diagnosis. Three of these four lesions were undetectable on CT images, and one was near the joint of the head of the rib.

Interreviewer Agreement

κ values for the differentiation between benign and malignant foci were 0.343 for scintigraphic images, 0.678 for separate data sets of scintigraphic and CT images, and 0.762 for fused images. Interreviewer agreement for separate data sets and fused images was considered to be substantial.

ROC Analysis

The A_z for reviewer 1 was 0.589 (95% confidence interval: 0.470, 0.708) for scintigraphic images, 0.831 (95% confidence interval: 0.737, 0.925) for separate data sets of scintigraphic and CT images, and 0.947 (95% confidence interval: 0.901, 0.992) for fused images (Fig 6a). The A_z for reviewer 2 was 0.771 (95% confidence interval: 0.671, 0.871) for scintgraphic images, 0.885 (95% confidence interval: 0.810, 0.960) for separate data sets of scintigraphic and CT images, and 0.968 (95% confidence interval: 0.932, 1.003) for fused images (Fig 6b).

Discussion

Imaging modalities are commonly differentiated as providing either functional or anatomic information (10–14, 16,17,29). Bone scintigraphy is a well-accepted functional imaging method for uncovering a variety of bone lesions (1–5,30). However, differentiating between bone metastasis and a benign lesion may often be difficult (1,30). The location of lesions on SPECT/CT images provides useful information to help differentiate these two conditions (31). SPECT imaging is often insufficient for the precise localization of bone lesions; hence, correlation with anatomic images such as CT scans or MR images is often necessary to increase the specificity of scintigraphic findings (1).

There is little doubt in the minds of most nuclear medicine and radiology specialists that the fusion of images acquired with separate modalities can be a considerable help in guiding patient care (11,17). However, it is clear that fused images are not required for all imaging studies. Therefore, it is necessary to identify the clinical areas in which image fusion is most effective in influencing patient care and outcome (11).

To our knowledge, comparison of SPECT/CT fusion and side-by-side reading of SPECT and CT data has been the subject of few studies (32). The results of our study showed that the fused images led to an improved ability of reviewers to differentiate malignant from benign bone lesions. The information gained by SPECT and CT image fusion was greater than the sum of their individual contributions. Additional review of fused images allowed for the precise localization of abnormal radiotracer uptake and enabled observers to be more confident of the lesion characteristics. Fused images facilitated the differentiation of benign from metastatic foci that were difficult to differentiate on scintigraphic and CT images viewed side by side. We found that fused images were especially useful for differentiating osteoarthritis. Metastatic foci that represented slight changes and that were overlooked on two separate sets of scin-
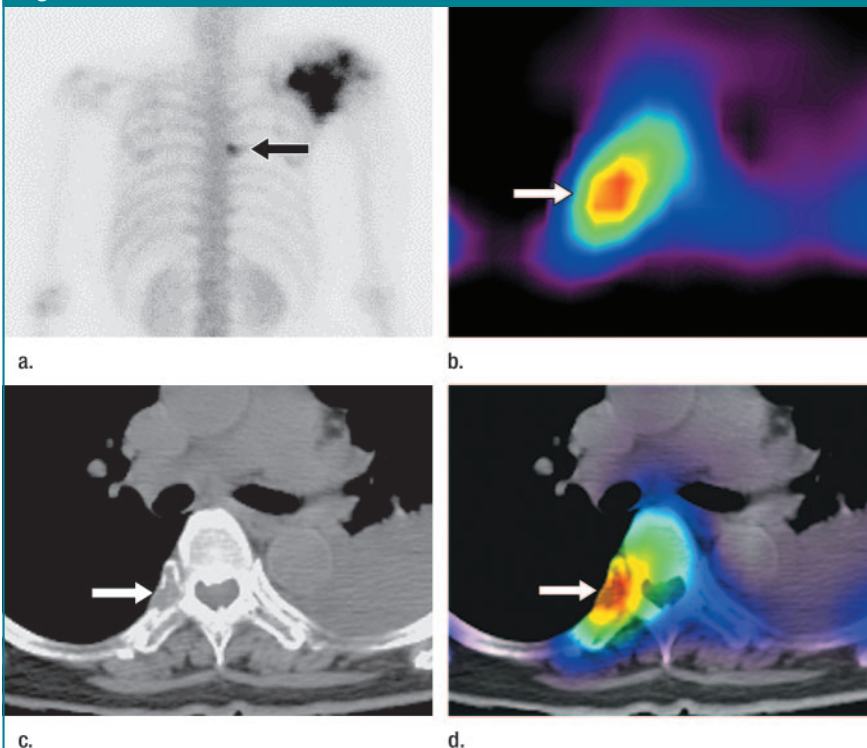
Figure 5

Figure 5: Images of 66-year-old woman with osteosarcoma of the scapula. **(a)** Posterior planar scintigram and **(b)** transverse SPECT image show a focus of increased tracer uptake near joint of the head of the rib (arrow). **(c)** Transverse CT image shows a small osteolytic site in head of the rib (arrow). **(d)** Transverse fused image shows abnormal radiotracer uptake in the osteolytic site (arrow). This finding on fused image was suggestive of bone metastasis. Later bone scans and CT scans helped confirm the bone metastasis.

tigraphic and CT images could be detected on fused images. An additional benefit of fused images is that spatially registered SPECT and CT images can be used to generate attenuation maps to correct attenuation errors in SPECT images (10,24,33–35). We believe the extra radiation can be justified if the CT scans were used not only for image fusion but also for attenuation correction purposes.

False-negative interpretations of fused images in our study were the result of a metastatic lesion located near the articulation or a metastatic lesion being undetectable on CT images. These false-negative cases are pitfalls in image interpretation of bone lesions. Abnormal foci near the articulations on bone scintigrams should be carefully interpreted. Positive bone scintigrams that showed findings not detected on CT images might require intensive follow-up studies or MR imaging.

Our study had several limitations. First, a detailed histopathologic analysis was not possible. We confirmed bone metastasis on the basis of radiologic studies and the subsequent clinical course. Second, we excluded patients who had more than five foci of abnormal radiotracer uptake. A large number (five or more) of abnormal foci was more likely to represent bone metastases (1). We considered that, in such cases, there was little need for formal registration or acquisition of a combined scan. This may have influenced the diagnostic performance and interobserver agreement for bone scintigraphy. Reviewer 2 was more experienced in interpretation of nuclear medicine images than was reviewer 1, which may also have contributed to the poor interobserver agreement for scintigraphic images alone. Third, potential registration errors in the thorax were due to breathing. Because a SPECT scan is an image created with data acquired over many breathing cycles, the fusion of SPECT images with CT images would require respiratory gating of the SPECT scan. However, this is not a promising approach owing to the substantial resultant increase in imaging time. In our study, it was feasible to achieve reason-

able image fusion in the thorax region in all cases. Fourth, a combined SPECT/CT system is not commonly used owing to its increased cost and comparative lack of availability. Moreover, we performed image fusion manually, and we confirmed the fusion by means of consensus of two radiologists. This is a time-consuming procedure that might limit the routine use of this technique. In recent years, there has been considerable progress in the development of fusion software to coregister different imaging modalities (17). Improved software algorithms are imperative to enable automatic and robust image fusion.

In conclusion, fusion of bone SPECT and CT scans offers an important advantage over assessment of two separate data sets for improved anatomic localization of a suspected site of increased radiotracer uptake at bone scanning. This provides increased diagnostic confidence in differentiating between malignant and benign lesions when analyzing findings of scans performed in oncologic patients.

References

1. Rybak LD, Rosenthal DI. Radiological imaging for the diagnosis of bone metastases. Q J Nucl Med 2001;45:53–64.
2. Savelli G, Maffioli L, Maccauro M, De Deckere E, Bombardieri E. Bone scintigraphy and the added value of SPECT (single photon emission tomography) in detecting skeletal lesions. Q J Nucl Med 2001;45:27–37.
3. Love C, Din AS, Tomas MB, Kalapparambath TP, Palestro CJ. Radionuclide bone imaging: an illustrative review. RadioGraphics 2003;23:341–358.
4. De Maeseneer M, Lenchik L, Everaert H, et al. Evaluation of lower back pain with bone scintigraphy and SPECT. RadioGraphics 1999;19:901–912.
5. Lynn MD, Braunstein EM, Wahl RL, Shapiro B, Gross MD, Rabbani R. Bone metastases in pheochromocytoma: comparative studies of efficacy of imaging. Radiology 1986;160:701–706.
6. Gayed I, Vu T, Johnson M, Macapinlac H, Podoloff D. Comparison of bone and 2-deoxy-2-[18F]fluoro-D-glucose positron emission tomography in the evaluation of bony metastases in lung cancer. Mol Imaging Biol 2003;5:26–31.
7. Yoshioka T, Yamaguchi K, Kubota K, et al. Evaluation of 18F-FDG PET in patients with advanced, metastatic, or recurrent gastric cancer. J Nucl Med 2003;44:690–699.
8. Duarte PS, Zhuang H, Castellucci P, Alavi A. The receiver operating characteristic curve for the standard uptake value in a group of patients with bone marrow metastasis. Mol Imaging Biol 2002;4:157–160.
9. Delpassand ES, Garcia JR, Bhadkamkar V, Podoloff DA. Value of SPECT imaging of the
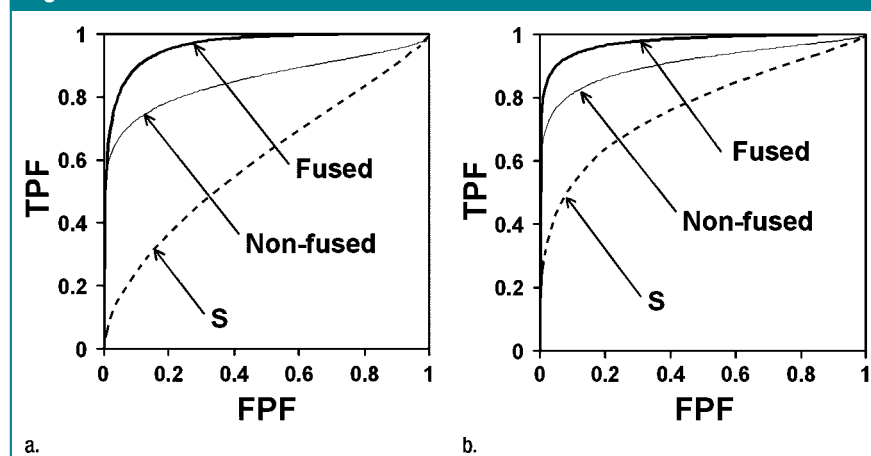

Figure 6: Graphs show ROC curves representing findings of scintigraphic image (dashed line), separate data sets of scintigraphic and CT images (thin solid line), and fused images (thick solid line). **(a)** ROC curve for reviewer 1; **(b)** ROC curve for reviewer 2. *FPF* = false-positive fraction, *S* = bone scintigraphic images alone, and *TPF* = true-positive fraction.

thoracolumbar spine in cancer patients. Clin Nucl Med 1995;20:1047–1051.

10. Bocher M, Balan A, Krausz Y, et al. Gamma camera-mounted anatomical x-ray tomography: technology, system characteristics and first images. Eur J Nucl Med 2000;27:619–627.

11. Cook GJ, Ott RJ. Dual-modality imaging. Eur Radiol 2001;11:1857–1858.

12. Kaplan IL, Swayne LC. Composite SPECT-CT images: technique and potential applications in chest and abdominal imaging. AJR Am J Roentgenol 1989;152:865–866.

13. Hasegawa BH, Wong KH, Iwata K, et al. Dual-modality imaging of cancer with SPECT/CT. Technol Cancer Res Treat 2002; 1:449–458.

14. Kramer EL, Noz ME, Sanger JJ, Megibow AJ, Maguire GQ. CT-SPECT fusion to correlate radiolabeled monoclonal antibody uptake with abdominal CT findings. Radiology 1989;172:861–865.

15. Zangheri B, Messa C, Picchio M, Gianolli L, Landoni C, Fazio F. PET/CT and breast cancer. Eur J Nucl Med Mol Imaging 2004; 31(suppl 1):S135–S142.

16. Israel O, Mor M, Gaitini D, et al. Combined functional and structural evaluation of cancer patients with a hybrid camera-based PET/CT system using (18)F-FDG. J Nucl Med 2002;43:1129–1136.

17. Townsend DW, Cherry SR. Combining anatomy and function: the path to true image fusion. Eur Radiol 2001;11:1968–1974.

18. von Schulthess GK. Positron emission tomography versus positron emission tomography/computed tomography: from "unclear" to "new-clear" medicine. Mol Imaging Biol 2004;6:183–187.

19. Miyake H, Matsumoto A, Hori Y, et al. War-thin's tumor of parotid gland on Tc-99m per-technetate scintigraphy with lemon juice stimulation: Tc-99m uptake, size, and pathologic correlation. Eur Radiol 2001;11:2472–2478.

20. Horiuchi M, Yasuda S, Shohtsu A, Ide M. Four cases of Warthin's tumor of the parotid gland detected with FDG PET. Ann Nucl Med 1998;12:47–50.

21. Shimizu A, Oriuchi N, Tsushima Y, Higuchi T, Aoki J, Endo K. High [18F] 2-fluoro-2-deoxy-D-glucose (FDG) uptake of adrenocortical adenoma showing subclinical Cushing's syndrome. Ann Nucl Med 2003;17: 403–406.

22. Tamaki N, Morita K. Myocardial imaging using PET and SPECT [in Japanese]. Nippon Rinsho 1998;56:2550–2555.

23. Bombardieri E, Seregni E, Villano C, Chiti A, Bajetta E. Position of nuclear medicine techniques in the diagnostic work-up of neuroendocrine tumors. Q J Nucl Med Mol Imaging 2004;48:150–163.

24. Kashiwagi T, Yutani K, Fukuchi M, et al. Correction of nonuniform attenuation and image fusion in SPECT imaging by means of separate x-ray CT. Ann Nucl Med 2002;16: 255–261.

25. Svanholm H, Starklint H, Gundersen HJ, Fabricius J, Barlebo H, Olsen S. Reproducibility of histomorphologic diagnoses with special reference to the kappa statistic. APMIS 1989;97:689–698.

26. DeLong ER, DeLong DM, Clarke-Pearson DL. Comparing the areas under two or more correlated receiver operating characteristic curves: a nonparametric approach. Biometrics 1988;44:837–845.

27. Efron B, Halloran E, Holmes S. Bootstrap confidence levels for phylogenetic trees. Proc Natl Acad Sci U S A 1996;93:13429–13434.

28. Rutter CM. Bootstrap estimation of diagnostic accuracy with patient-clustered data. Acad Radiol 2000;7:413–419.

29. Even-Sapir E, Keidar Z, Sachs J, et al. The new technology of combined transmission and emission tomography in evaluation of endocrine neoplasms. J Nucl Med 2001;42: 998–1004.

30. Gates GF. SPECT bone scanning of the spine. Semin Nucl Med 1998;28:78–94.

31. Even-Sapir E, Martin RH, Barnes DC, Pringle CR, Iles SE, Mitchell MJ. Role of SPECT in differentiating malignant from benign lesions in the lower thoracic and lumbar vertebrae. Radiology 1993;187:193–198.

32. Reinartz P, Wieres FJ, Schneider W, Schur A, Buell U. Side-by-side reading of PET and CT scans in oncology: which patients might profit from integrated PET/CT? Eur J Nucl Med Mol Imaging 2004;31:1456–1461.

33. Delbeke D, Martin WH, Patton JA, Sandler MP. Value of iterative reconstruction, attenuation correction, and image fusion in the interpretation of FDG PET images with an integrated dual-head coincidence camera and x-ray-based attenuation maps. Radiology 2001;218:163–171.

34. Dey D, Slomka PJ, Hahn LJ, Kloiber R. Automatic three-dimensional multimodality registration using radionuclide transmission CT attenuation maps: a phantom study. J Nucl Med 1999;40:448–455.

35. LaCroix KJ, Tsui BM, Hasegawa BH, Brown JK. Investigation of the use of x-ray CT images for attenuation compensation in SPECT. IEEE Trans Nucl Sci 1994;41:2793–2799.